

Article

Application of the NO_x Reaction Model for Development of Low-NO_x Combustion Technology for Pulverized Coals by Using the Gas Phase Stoichiometric Ratio Index

Masayuki Taniguchi *, Yuki Kamikawa, Tsuyoshi Shibata, Kenji Yamamoto and Hironobu Kobayashi

Energy and Environmental Systems Laboratory, Hitachi, Ltd. Power Systems Company, 7-2-1 Omika-cho, Hitachi-shi, Ibaraki-ken, 319-1292, Japan;

E-Mails: yuki.kamikawa.cg@hitachi.com (Y.K.); tsuyoshi.shibata.ae@hitachi.com (T.S.); kenji.yamamoto.va@hitachi.com (K.Y.); hironobu.kobayashi.gh@hitachi.com (H.K.)

* Author to whom correspondence should be addressed;

E-Mail: masayuki.taniguchi.xc@hitachi.com; Tel.: +81-29-276-5889.

Received: 9 December 2010; in revised form: 14 February 2011 / Accepted: 16 March 2011 / Published: 23 March 2011

Abstract: We previously proposed the gas phase stoichiometric ratio (SR_{gas}) as an index to evaluate NO_x concentration in fuel-rich flames. The SR_{gas} index was defined as the amount of fuel required for stoichiometric combustion/amount of gasified fuel, where the amount of gasified fuel was the amount of fuel which had been released to the gas phase by pyrolysis, oxidation and gasification reactions. In the present study we found that SR_{gas} was a good index to consider the gas phase reaction mechanism in fuel-rich pulverized coal flames. When $SR_{gas} < 1.0$, NO_x concentration was strongly influenced by the SR_{gas} value. NO_x concentration was also calculated by using a reaction model. The model was verified for various coals, particle diameters, reaction times, and initial oxygen concentrations. The most important reactions were gas phase NO_x reduction reactions by hydrocarbons. The hydrocarbon concentration was estimated based on SR_{gas} . We also investigated the ratio as an index to develop a new low-NO_x combustion technology for pulverized coals. We examined the relation between local SR_{gas} distribution in the fuel-rich region in the low-NO_x flame and NO_x emissions at the furnace exit, by varying burner structures. The relationship between local SR_{gas} value and local NO_x concentration was also examined. When a low-NO_x type burner was used, the value of SR_{gas} in the flame was readily decreased. When the local SR_{gas} value was the same, it was difficult to influence the local

NO_x concentration by changing the burner structure. For staged combustion, the most important item was to design the burner structure and arrangement so that SR_{gas} could be lowered as much as possible just before mixing with staged air.

Keywords: low- NO_x combustion; pulverized coals; NO_x reduction; gas phase stoichiometric ratio; hydrocarbons

Nomenclature:

E : activation energy (J/mol);	SR_{in} : inlet stoichiometric ratio;
k : frequency factor;	SR_{gas} : gas phase stoichiometric ratio;
L : distance between the burner nozzle and sampling port (mm);	T : gas temperature (K);
n : constant;	X : axial location (mm);
$[\text{NO}_x]$: concentration of NO_x (mol/m^3);	X_{CO} : mole fraction of carbon monoxide;
$[\text{OH}]$: concentration of OH (mol/m^3);	X_{CH_4} : mole fraction of methane;
$[\text{OH}_{eq}]$: equilibrium concentration of OH (mol/m^3);	X_{H_2} : mole fraction of hydrogen;
$\text{Ox}(\text{OH})$: oxidative species, such as OH;	X_{O_2} : mole fraction of oxygen;
P_{O_2} : partial pressure of oxygen (Pa);	$X_{\text{O}_2 0}$: mole fraction of oxygen in combustion supporting gas;
P_{CO_2} : partial pressure of carbon dioxide (Pa);	XN (NH_3 , HCN): nitrogenous species;
$P_{\text{H}_2\text{O}}$: partial pressure of water (Pa);	$[\text{XN}]$: concentration of XN (mol/m^3);
R : gas constant, 8.314 J/K mol;	$[\text{XNradical}]$: concentration of XNradical (mol/m^3);
S : total surface area of coal or char (m^2/kg -total gas);	X_{THC} : mole fraction of total hydrocarbons;
S' : total surface area of coal or char (m^2/m^3 -total gas);	X_{TR} : mole fraction of tracer;
	$X_{\text{TR} 0}$: mole fraction of tracer in combustion supporting gas

1. Introduction

The implementation of low- NO_x -combustion technologies for pulverized coals began in the 1980s [1]. Low NO_x combustion technologies have included two-stage combustion [2], re-burning [2,3], and in-flame NO_x reduction by using a low- NO_x burner [1,4]. A feature which is common to all these technologies is that the NO_x reduction region was formed in the flame where the oxygen concentration was very low [1]. To predict NO_x emissions well, it is important to be able to reliably predict NO_x concentrations in the NO_x reduction region. However, for combustion of coal, NO_x reduction performance changes easily with the burning conditions, such as coal properties [3] and coal particle diameter. However, boiler design and development cannot be done efficiently if it is necessary to change the method of NO_x reduction for each coal property. In a previous study, we proposed an index to estimate NO_x reduction performance [5]. This index has hardly any influence from the burning conditions. In the present study, we introduce a case which utilizes the proposed index to develop a new low- NO_x -combustion technology.

As computers have become even more sophisticated, their use to perform the numerical analyses needed in designing pulverized coal firing boilers is increasing [6–11]. The reduction of the computational load is important for engineering design of actual boilers, and this can be done by using appropriate models based on our proposed index.

Several studies have been made to investigate the reaction of volatile matter [12,13]. These studies focused on the first half of the coal combustion phenomenon. Other studies have focused on the second half of the coal combustion, the char combustion region [14,15]. While studies on NO_x reduction by char [16–19] have been made, the contribution for total NO_x emission from the pulverized coal combustion was not clear. In previous studies, we proposed a NO_x reaction model which focused on the gas phase reaction in the char combustion region [5,15]. A key reaction was reduction of NO_x by hydrocarbons. In the present study, the model was verified for various coals, particle diameters, reaction times, and initial oxygen concentrations.

2. Results and Discussion

2.1. The Relationship between Gas Phase Stoichiometric Ratio, SR_{gas} , and NO_x

Previously, we evaluated NO_x generation characteristics for the fuel-rich condition in an experiment which used a drop-tube furnace [15]. Under these conditions the NO_x characteristics seemed to depend on the burning conditions. Then, we analyzed the experimental data in the relationship between inlet stoichiometric ratio (SR_{in}) and NO_x and this result depended on the coal properties, particle diameter, and burning temperature. SR_{in} was defined as the stoichiometric ratio of inlet mixture of coal and air as shown in Equation (1) [5]:

$$SR_{in} = \text{amount of fuel required for stoichiometric combustion/amount of fuel actually supplied} \quad (1)$$

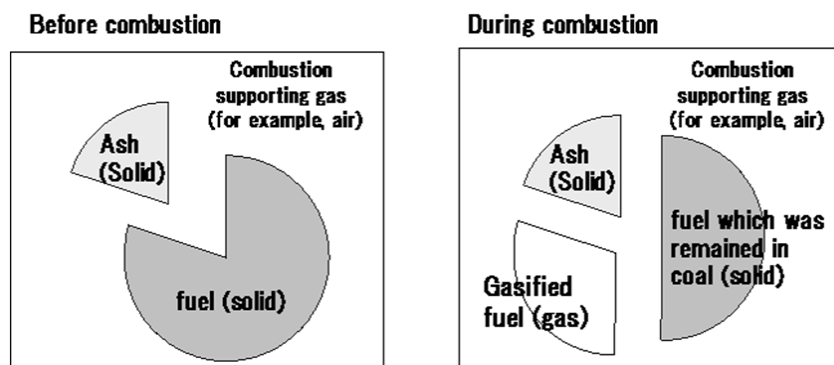
For pulverized coal combustion NO_x is reduced by both gas phase and solid phase reactions [5,15]. We tried to analyze the experimental data in reference [15] by separating them into gas phase and solid phase reactions; we focused especially on the gas phase reaction.

Figure 1 shows how to obtain the value of SR_{gas} . Before combustion, all fuel components of the pulverized coals are in the solid phase. Pulverized coal particles are surrounded by a combustion supporting gas such as air.

After the coal particles are ignited, some of the fuel components move from the solid phase to the gas phase by pyrolysis, oxidation, and gasification reactions (Figure 1). The remaining fuel components stay in the solid phase. The gas phase stoichiometric ratio is the index which focuses on the amount of fuel components moving from the solid phase to the gas phase. We define the gas phase stoichiometric ratio (SR_{gas}) by Equation (2):

$$SR_{gas} = \text{amount of fuel required for stoichiometric combustion/amount of gasified fuel} \quad (2)$$

Here, the amount of gasified fuel means both the amount of fuel that has moved from the solid phase to the gas phase by pyrolysis, oxidation, and gasification reactions, and, the amount of gas and liquid fuel supplied to the combustible mixture. We do not consider the fuel components which are left in the solid phase.

Figure 1. Definition of gas phase stoichiometric ratio (*SRgas*).

Usually, the gas phase reaction rate exceeds the solid phase reaction rate. When the gas phase reaction is the focus, sometimes the effect of the solid phase reaction can be ignored. The stoichiometric ratio is a good index which shows the difference in the burning conditions. We thought a numerical analysis might become easy when solid is removed from the burning mixture and an equivalence ratio is defined to consider the gas phase reaction.

The *SRgas* index can be obtained by analyzing the mass balance of H, C and O in the burning gas. Sometimes, it is difficult to analyze the mass balance correctly, because the amount of water is difficult to measure. For such a situation, *SRgas* can be approximately by Equation (3):

$$SR_{gas} = \frac{X_{O_2} / X_{TR0}}{X_{O_2,0} / X_{TR0} - X_{O_2} / X_{TR} + 0.5X_{CO} / X_{TR} + 0.5X_{H_2} / X_{TR} + 2X_{CH_4} / X_{TR}} \quad (3)$$

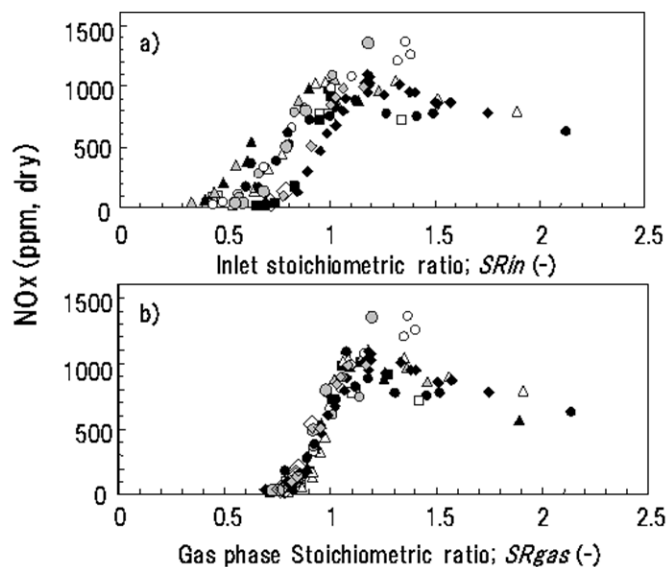
Here, X_{O_2} , X_{CO} , X_{H_2} , and, X_{CH_4} are O_2 , CO , H_2 , and CH_4 mole fractions in the burning gas. $X_{O_2,0}$ is the average mole fraction of O_2 in the combustion supporting gas. X_{TR} is the concentration of tracer. N_2 , Ar and He are examples of suitable tracers. In the present study, we chose N_2 as a tracer because there is hardly any change in its amount due to chemical reactions. X_{TR0} is the concentration of tracer in the combustion supporting gas.

At first, combustible materials in the coal are released to the gas phase as CO , hydrocarbons and H_2 . When the gas contains sufficient oxygen the CO , hydrocarbons, and H_2 are oxidized by O_2 to form CO_2 and H_2O , respectively. When the gas contains little oxygen, a part of CO , hydrocarbon and H_2 remain in the gas. The quantity of the fuel that was moved from the solid phase to gas phase could be estimated by measuring the amount of O_2 , CO , hydrocarbon and H_2 in the gas. The concentration of CH_4 was mentioned specifically in Equation (3) because CH_4 was the major hydrocarbon remaining in flames.

Figure 2 plots the NO_x concentration characteristics obtained for the drop-tube furnace [15]. The results were obtained for a variety of coal properties (these are summarized later in Table 1), particle diameters, burning temperatures, and compositions of combustion supporting gas. Relationships between both *SRin* and NO_x , and *SRgas* and NO_x are shown in the figure. When the data were analyzed by *SRin*, NO_x concentration varied with experimental conditions. However, when the data were analyzed by *SRgas* the difference between NO_x concentrations became small and NO_x was barely influenced by the burning conditions when *SRgas* was less than 1.0. We judged that *SRgas* was a good

index which estimated NO_x concentration in fuel-rich conditions. We further thought that the gas phase NO_x reduction was the key reaction when SR_{gas} was smaller than 1.0; that is, the mechanism of the gas reaction did not depend so much on properties of the coal and there were many common points.

Figure 2. Relationship between gas phase stoichiometric ratio and NO_x concentration.

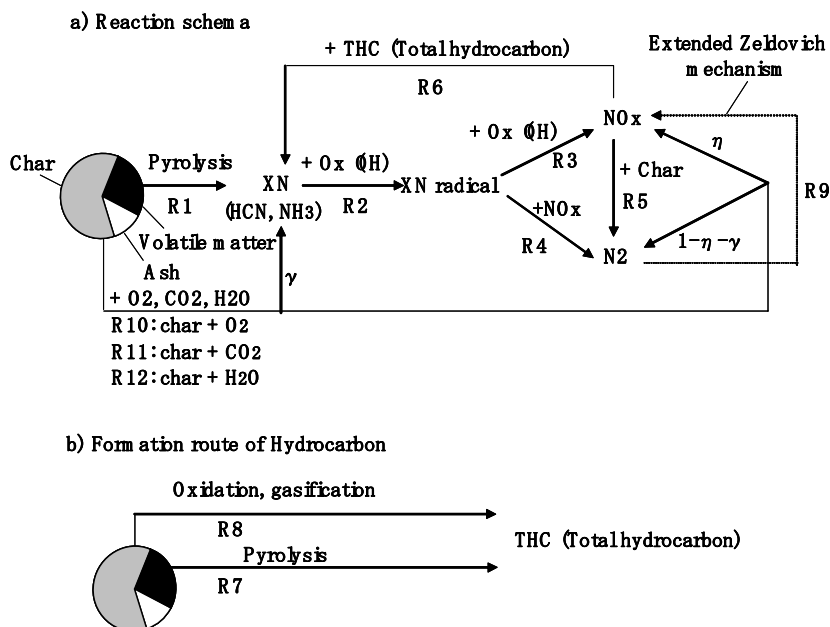


Symbol	Coal	Temp. (K)	Combustion Supporting Gas	Inlet O_2 (vol%)	Diameter (μm)	L (mm)
◆	A	1673	air	21	40	800
◇	B	1573	air	21	59	800
■	C	1573	air	21	17	800
△	D	1573	air	21	37	800
▲	D	1573	air	21	37	200–400
▲	D	1673	CO_2/O_2	21	37	800
○	F	1673	air	21	45	800
●	F	1673	N_2/O_2	16	45	800
●	F	1673	N_2/O_2	24	45	800
□	J	1673	air	21	16	800
◇	K	1873	air	21	45	800

2.2. Reaction Model

Previously, we proposed a NO_x reaction model which can estimate NO_x concentrations under fuel-rich conditions [5]. The main reaction scheme is shown in Figure 3. The main feature of the model is the gas phase reaction of NO_x reduction by hydrocarbons. $\text{Ox}(\text{OH})$ is an important oxidative species. We thought that concentrations of hydrocarbons and $\text{Ox}(\text{OH})$ strongly depend on SR_{gas} . According to the scheme, NO_x is mainly reduced by hydrocarbons to form XN (NH_3 , HCN). Most of the XN (NH_3 , HCN) forms NO_x again. However, the remaining XN reacts with NO_x to form N_2 . Reactions used for this study are listed in Table 1. $(\text{H}/\text{C})_{\text{VM}}$ in Table 1 is molar ratio of H and C in volatile matter. $(\text{H}/\text{C})_{\text{char}}$ in Table 1 is molar ratio of H and C in char. Example of $(\text{H}/\text{C})_{\text{VM}}$ and $(\text{H}/\text{C})_{\text{char}}$ values were described elsewhere [15].

Figure 3. Reaction model of NO_x formation and reduction.



We estimated total hydrocarbons THC in the following way: hydrocarbons are mainly formed from the part of the fuel which was released from the solid phase to the gas phase by the pyrolysis, oxidation, and gasification reactions. We assumed that the amount of THC formation increases with the rates of these reactions. Hydrogen is necessary for THC formation. When the hydrogen content in a solid fuel is increased, the THC formation rate increases. It is easy to form THC in the volatile combustion region, because more hydrogen is contained in the volatile matter than in the char. Finally, we concluded that *SRgas* was the most important factor.

Table 1. Reactions used in this study.

No.	Reaction	Form
R1	Pyrolysis of volatile matter	See Ref. 20
R2	XN + OH → XNradical	$d[XN]/dt = k_{R2} \exp(-E_{R2}/RT) [XN][OH]$
R3	XNradical + OH → NO _x	$d[XNradical]/dt = k_{R3} \exp(-E_{R3}/RT) [XNradical][OH]$
R4	XNradical + NO _x → N ₂	$d[XNradical]/dt = k_{R4} \exp(-E_{R4}/RT) [XNradical][NO_x]$
R5	NO _x + Char → N ₂	$d[NO_x]/dt = k_{R5} \exp(-E_{R5}/RT) S' [NO_x]^n$
R6	NO _x + THC → N ₂ + XN	$d[NO_x]/dt = k_{R6} \exp(-E_{R6}/RT) [NO_x][THC]$
R9	Extended Zelvovich mechnism	
R10	C + 0.5O ₂ → CO	$dC/dt = k_{R10} \exp(-E_{R10}/RT) S P_{O_2}^n$
R11	C + CO ₂ → 2CO	$dC/dt = k_{R11} \exp(-E_{R11}/RT) S P_{CO_2}^n$
R12	C + H ₂ O → CO + H ₂	$dC/dt = k_{R12} \exp(-E_{R12}/RT) S P_{H_2O}^n$
Estimation of Total Hydrocarbon concentration		$X_{THC} = k_{THC}((H/C)_{VM} R1 + (H/C)_{char} (R10 + R11 + R12)) (1/SRgas)^n \exp(-E_{THC}/RT)$

The steady state assumption was used for reactions of XNradical. For R3 and R4, the ratio of the reaction rates (R3/R4) is important. A pyrolysis model was proposed by Yamamoto *et al.* [20]. The concentration of OH was calculated by using equilibrium concentration and gas temperature. Equation (4) proposed by Bose and Wendt [14] was used for the calculations:

$$[\text{OH}] = 1.3 \times 10^4 \exp(13000/T) \times [\text{OH}_{\text{eq}}] \quad (4)$$

Reaction parameters are listed in Tables 2 and 3. Table 2 shows parameters of solid phase reactions of coal K (hv-bituminous coal). These parameters vary with coal properties. Usually, the rate constants of R5, R10, R11, and R12 are decreased with fuel-ratio. The rate constant of R5 was estimated from char combustion experiments [15]. Char was burnt in N₂-O₂-NO mixtures. O₂ in the surrounding gas was varied from 2 to 9 vol %. NO in the surrounding gas was varied from 0 to 512 ppm. The rate constants were estimated by difference of the NO concentration between inlet and exit value. For some coals, the values of k_{R5} were varied with surrounding oxygen concentration. Values of γ and η in Figure 3 also varied with coal properties. For coal K, γ was 0.2 and η was 0.07.

Table 3 shows the gas phase reaction parameters. These parameters were the same for all coals. O₂, H₂, CO and CO₂ concentration in the drop-tube furnace were measured under various temperatures and stoichiometric ratios. Concentrations of these species could be similar by equilibrium values.

Table 2. Parameters of solid phase reactions.

Reaction	k	E	n
R5 (mol-NO/m ³ -total gas s)	$k_{R5} = 0.865 + 10.8 X_{O_2} ((\text{m}^3/\text{mol})^{0.9} \text{ m s}^{-1})$	28 (kJ/mol)	0.9
R10 (kg-carbon/kg-total gas s)	$7.99 \times 10^{-4} (\text{kg}/\text{m}^2 \text{ Pa s})$	66 (kJ/mol)	1
R11 (kg-carbon/kg-total gas s)	$1.46 \times 10^{-3} (\text{kg}/\text{m}^2 \text{ Pa s})$	154 (kJ/mol)	1
R12 (kg-carbon/kg-total gas s)	$1.46 \times 10^{-2} (\text{kg}/\text{m}^2 \text{ Pa s})$	154 (kJ/mol)	1
X _{THC} (mole fraction, as CH ₄)	$3.15 \times 10^{-9} (\text{kg-total gas s}/\text{kg-carbon})$	-195 (kJ/mol)	13

Table 3. Parameters of gas phase reactions.

Reaction	k	E
R2 (mol/m ³ s)	$4.6899 \times 10^6 (\text{m}^3/\text{mol s})$	43.2 (kJ/mol)
R3 (mol/m ³ s)	$5.35 \times 10^{10} (\text{m}^3/\text{mol s})$	168 (kJ/mol)
R4 (mol/m ³ s)	$1.52 \times 10^{12} (\text{m}^3/\text{mol s})$	251 (kJ/mol)
R5 (mol/m ³ s)	$1.64 \times 10^{15} (\text{m}^3/\text{mol s})$	372 (kJ/mol)

2.3. Calculated Results

Figures 4, 5 and 6 show verifications of the calculation model using the experimental results obtained with the drop-tube furnace. Figure 4 shows the effect of coal properties (see Table 4 below) and burning temperature on NO_x concentration. We checked the results for both the relationships between *SR_{in}* and NO_x, and *SR_{gas}* and NO_x. The calculated results reproduced both characteristics. When *SR_{gas}* was less than 1.0, NO_x was influenced by *SR_{gas}*, while it was hardly influenced at all by the other experimental conditions.

We checked the model for around 200 other experimental conditions. We changed oxygen and NO_x concentrations in the combustion supporting gas, particle diameters, and burning times ($L = 400\text{--}800$ mm). The results are shown in Figure 5. The difference between experimental and calculated results was approximately 20%. When particle size was very large, calculation precision decreased. The calculation did not predict the value of *SR_{gas}* well, because the calculation error of the coal burnout became large. At first, it is important to predict the value of *SR_{gas}* well, for predicting NO_x concentration well.

Figure 4. Effect of coal properties and burning temperature on NO_x concentration, symbols are experimental results and lines are calculated results.

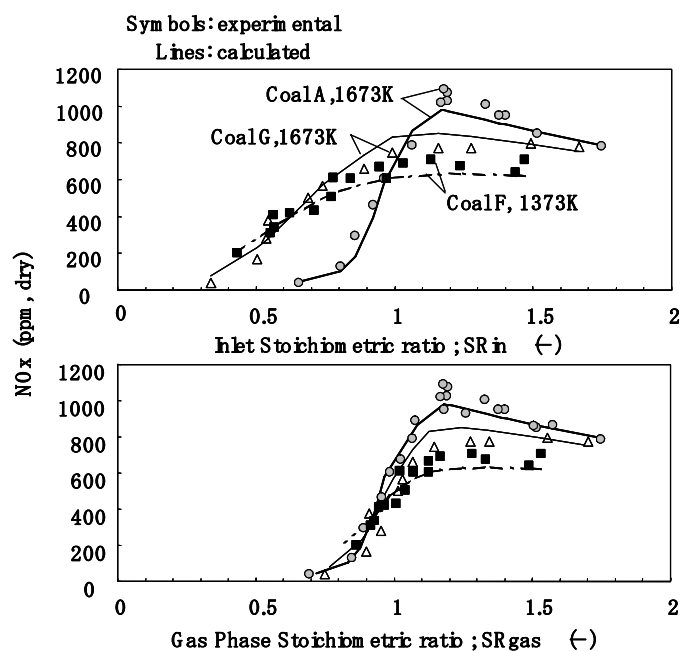
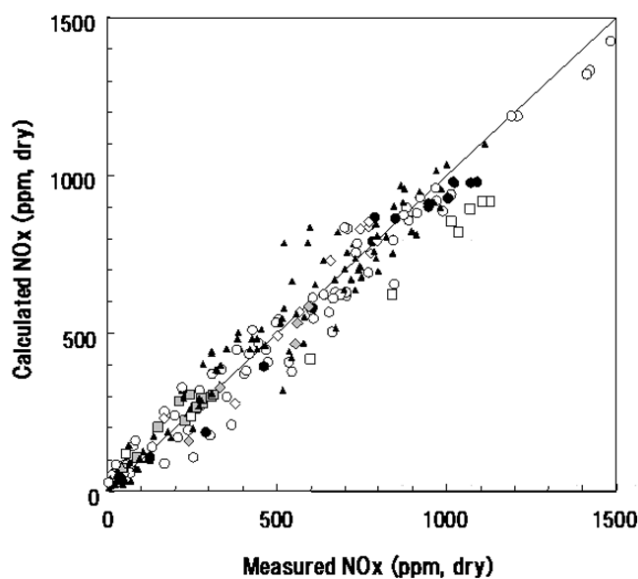


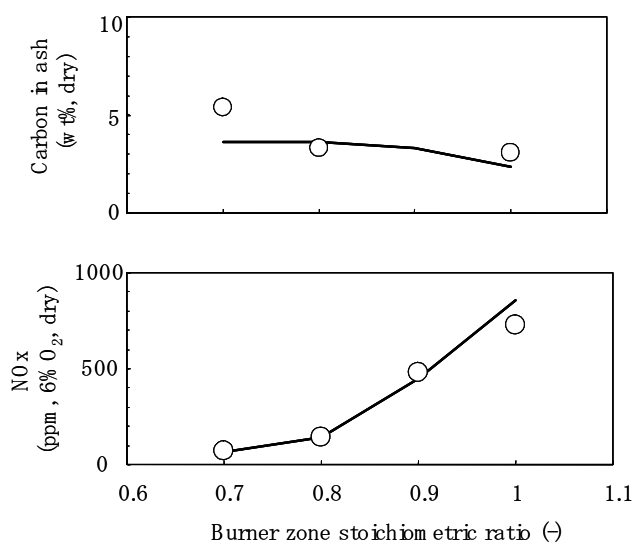
Figure 5. Comparison between measured (symbols) and calculated (line) NO_x concentrations.



Symbol	Coal	Temp. (K)	Inlet O ₂ (vol%)	Inlet NO _x (ppm)	Diameter (μm)	L (mm)
●	A	1673	21	0	40	800
▲	B	1173–1773	21	0	23–155	400–800
□	E	1673	21	0	22	800
○	F	1173–1673	16–24	0–1000	14–45	800
◇	G	1673	21	0	40	800
◆	H	1673	21	0	33	800
■	I	1673	21	0	35	800

Staged combustion properties were also verified for coal K. Typical results are shown in Figure 6. Structures of the drop-tube furnace for staged combustion are shown later (Figure 16). Burning temperatures of these experiments were higher than those shown in Figure 4 and 5. NO_x concentration and carbon in ash were measured at the furnace exit. The proposed model was also verified for staged combustion conditions.

Figure 6. Staged combustion properties of coal K. Exit stoichiometric ratio was 1.2. Burning temperature was 1873 K for the burner zone and 1673 K for the staged combustion zone. Residence time was around 1.4 s for the burner zone and around 1.0 s for the staged combustion zone. Symbols are experimental and lines are calculated results.



2.4. Application of SRgas to Low- NO_x -Combustion Technology Development in the Air Combustion Experiment

Structures of the laboratory scale furnace for the air combustion experiment are shown in Figure 7 [1]. The furnace was the down flow type combustor, in which pulverized coal particles and air were supplied from the upper part of the apparatus. The combustion air was divided into the primary (1ry), secondary (2ry) and ternary (3ry) air. Coal feed rate was approximately 25 kg/h. Pulverized coals were supplied through the primary air nozzle. Burner Nozzles A and B structures are shown in Figure 8. The structure of the third Nozzle C was the same as that of Nozzle B, but the angles of their swirler vanes were different. The nozzles used the swirler vane to form a swirled flow, and plate-like members to obtain a straight flow. The effects of the swirler vane and the plate-like members were described previously [21]. In the present study, we tested NO_x emission by varying the diameter of the primary nozzle, the size of the swirler vane and the plate-like members, and the angle of the swirler vane.

Figure 9 shows the relationship between burner stoichiometric ratio and NO_x emission obtained for the three nozzles. Coal E (see Table 1) was used for these experiments. NO_x emission using Nozzle B was the lowest, followed by Nozzle A and Nozzle C.

Figure 7. Schematic diagram of the laboratory scale furnace (unit: mm).

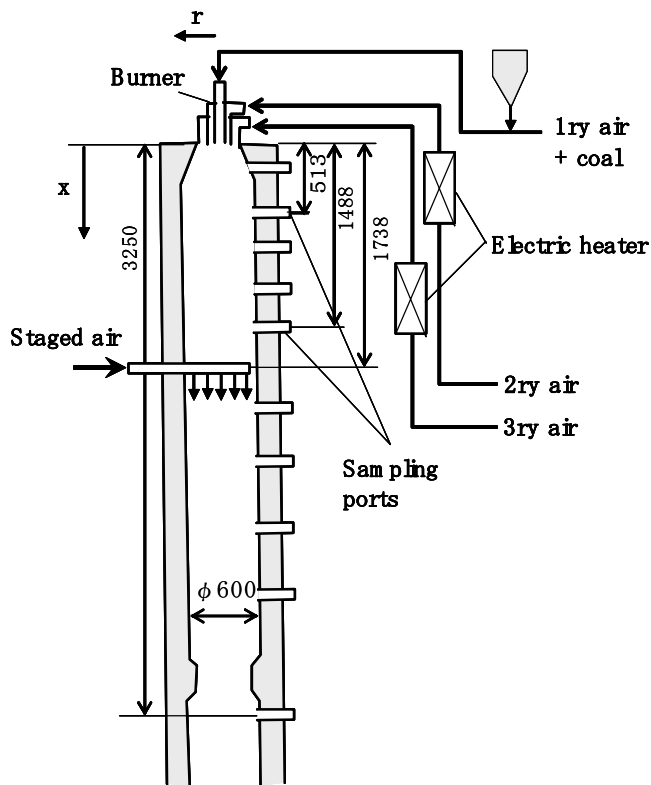


Figure 8. Structure of burner and nozzles (unit: mm).

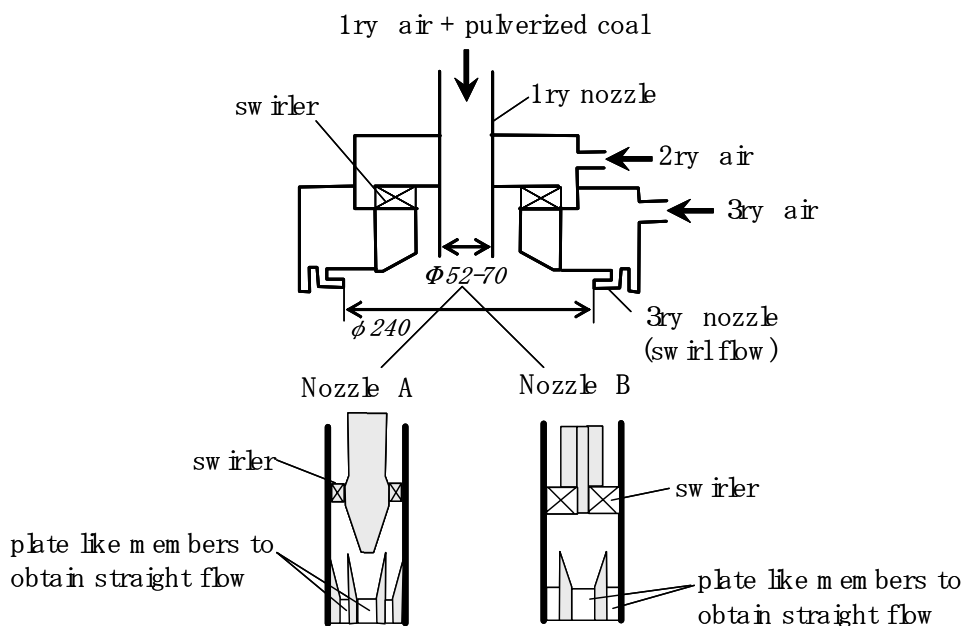
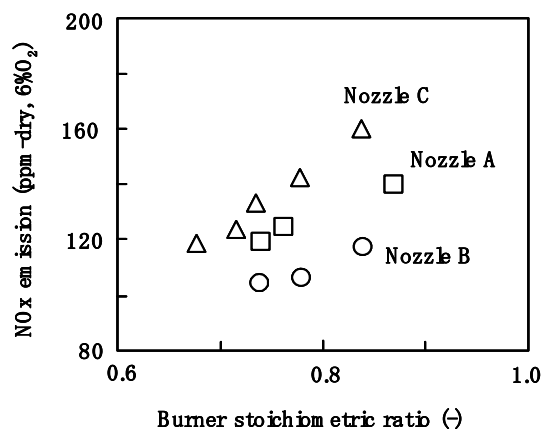
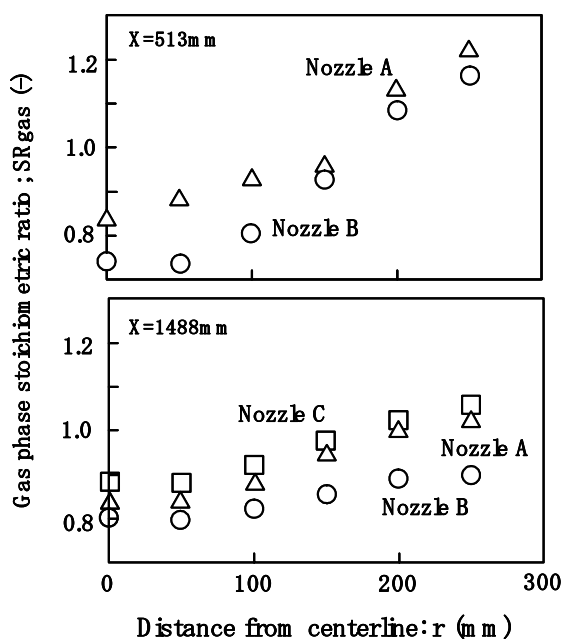


Figure 9. Comparison of NO_x emissions for three burner structures at different stoichiometric ratios. Exit stoichiometric ratio was 1.15 for all experiments (exit O₂ was 2.7 vol%, dry).



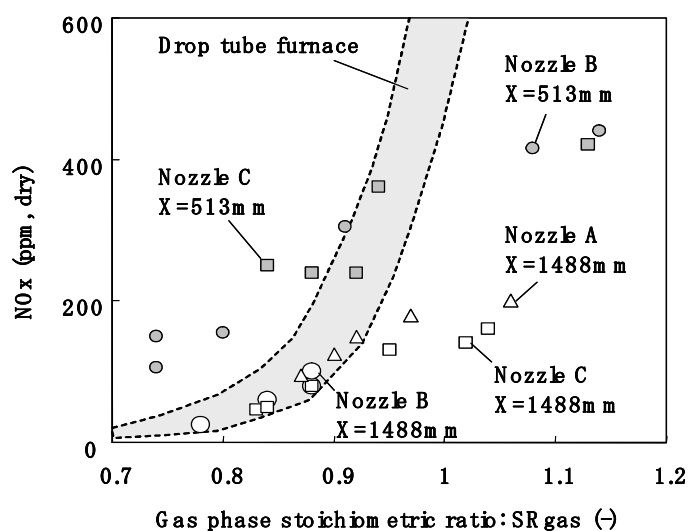
We measured local *SRgas* distributions in the flames and the results are shown in Figure 10. Local *SRgas* distributions were measured at two different axial positions. One was obtained in the burner neighborhood ($x = 513$ mm) and the other was obtained just before the staged air nozzle ($x = 1488$ mm). *SRgas* had the minimum value at the central axis, and it increased near the side wall of the furnace. Then we investigated the effect of nozzle structure on *SRgas*. When we used the low-NO_x type Nozzle B, the value of *SRgas* was easily decreased. The same characteristics were observed at both $X = 513$ mm and $X = 1488$ mm. *SRgas* was also a good index for investigating the reason why NO_x emissions were reduced. When the NO_x concentration was compared for the same axial position, the NO_x concentration was strongly influenced by *SRgas*, but hardly influenced by the nozzle structure. The key to low NO_x combustion technology development is reducing the value of *SRgas* in the burner zone as much as possible.

Figure 10. Distribution of gas phase stoichiometric ratio for the laboratory scale furnace.



The relationship between SR_{gas} and NO_x concentration obtained in the drop-tube furnace is shown in Figure 11. We compared NO_x concentration obtained just before the staged air nozzle ($x = 1488$ mm). When SR_{gas} was less than 0.9, NO_x concentrations obtained by the laboratory scale furnace and drop-tube furnace were almost the same. NO_x concentration was made stable by SR_{gas} . NO_x emission was strongly influenced by how much the SR_{gas} value could be reduced just before staged air injection. The NO_x concentration in the vicinity of the burner ($x = 513$ mm) was higher than that obtained downstream ($x = 1488$ mm). The SR_{gas} was a good index to consider NO_x performance, but, in the burner neighborhood, it did not predict the actual value. We thought that one of the reasons was the concentration fluctuation. Flow turbulence could be strong in the burner neighborhood. This might cause concentration fluctuation. In the burner neighborhood, both reductive gas ($SR_{gas} < 1.0$) and oxidative gas ($SR_{gas} > 1.0$) conditions were observed at the same position. NO_x in oxidative gas was high, so that NO_x in the burner neighborhood became high, even if SR_{gas} was low.

Figure 11. Relationship between gas phase stoichiometric ratio and NO_x concentration for the laboratory scale furnace.

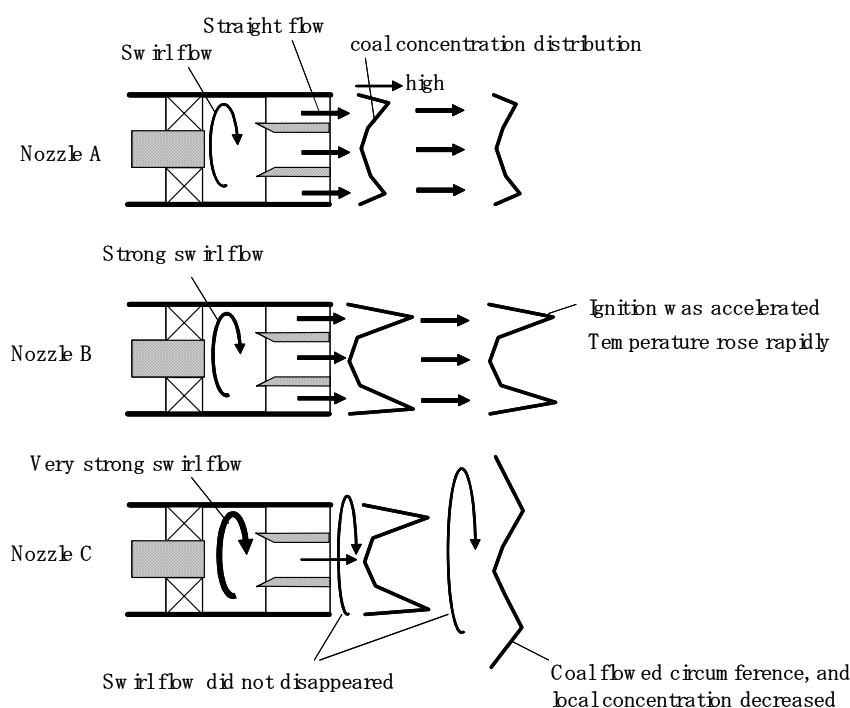


We examined why NO_x emissions varied with nozzle structures. Figure 12 shows differences in flow and coal concentration distributions near the burner exit between Nozzles A, B and C. Swirl flow was formed inside the nozzle. The local coal concentration of nozzle circumference rose by the centrifugal force of the swirl flow. The plate-like members installed at the nozzle exit changed swirl flow into straight flows. The resulting phenomenon was that local coal concentrations rose as the nozzle circumference side was maintained. The coals ignited from the circumference side of the nozzle. When the coal concentration rose, ignition was accelerated, then, the flame temperature rose rapidly. Oxidation and gasification reactions were accelerated because of high flame temperature, then, coal burnout in the burner zone easily increased. SR_{gas} value was easy to decrease, so NO_x concentration decreased.

The swirl strength of Nozzle B was larger than that of Nozzle A. Consequently the local coal concentration in the nozzle circumference of Nozzle B was larger than that of Nozzle A, and coal ignition in Nozzle B became easy.

The swirl strength of Nozzle C was very large, however, swirl ingredients were left at the nozzle exit. The coal particles which gathered in the nozzle circumference spread more on the circumference side. For Nozzle C, the local coal concentration at the nozzle exit could not kept high. Coal ignition was not accelerated.

Figure 12. Images of flow and coal concentration distributions near the burner exit for Nozzles A, B and C.



2.4. Application of SRgas to Low-NO_x-Combustion Technology Development in the Oxyfuel Combustion Calculation

We applied the model to the oxyfuel combustion calculation for a boiler. Two kinds of NO_x are formed from pulverized coal combustion, thermal NO_x and fuel NO_x. The SRgas mainly affects prediction of the fuel NO_x as most of the NO_x generated in oxyfuel combustion is fuel NO_x, because the combustion supporting gas only contains a little nitrogen.

We calculated NO_x emissions for a pulverized coal firing boiler. We used a boiler of average size and structure based on publicly available information [22–26] about recent pulverized coal firing power plants. The electric output was around 1000 MW. Figure 13 shows calculation conditions and example results for the calculated concentration distributions of O₂ and NO_x, and gas temperature distribution. The calculation method was shown previously [7,8]. NO_x near the burner neighborhood was high, where oxygen concentration and SRgas were high. The oxygen concentration and SRgas decreased at the center of the furnace where NO_x was reduced and the NO_x concentration increased a little by mixing with staged air.

The variations in SRgas in the furnace are shown in Figure 14. The SRgas distributions are expressed as an average for a horizontal section of the furnace. The SRgas depended on the burner arrangement. We compared the SRgas values just before mixing with staged air. The SRgas of Case 2

was lower than that of Case 1. NO_x emissions, O_2 concentration, and unburned carbon in fly-ash at the exit of the furnace are shown in the figure. Oxygen concentration and unburned carbon in fly-ash were equal. However, the NO_x emission of Case 2 was lower than that of Case 1. The SR_{gas} became lower just before mixing with staged air, and NO_x emission became lower. The results were the same as obtained from the experiments. In development of the low NO_x combustion technology, the SR_{gas} was a good index for investigating the mechanism of NO_x reduction.

Figure 13. Numerical calculation for oxyfuel combustion.

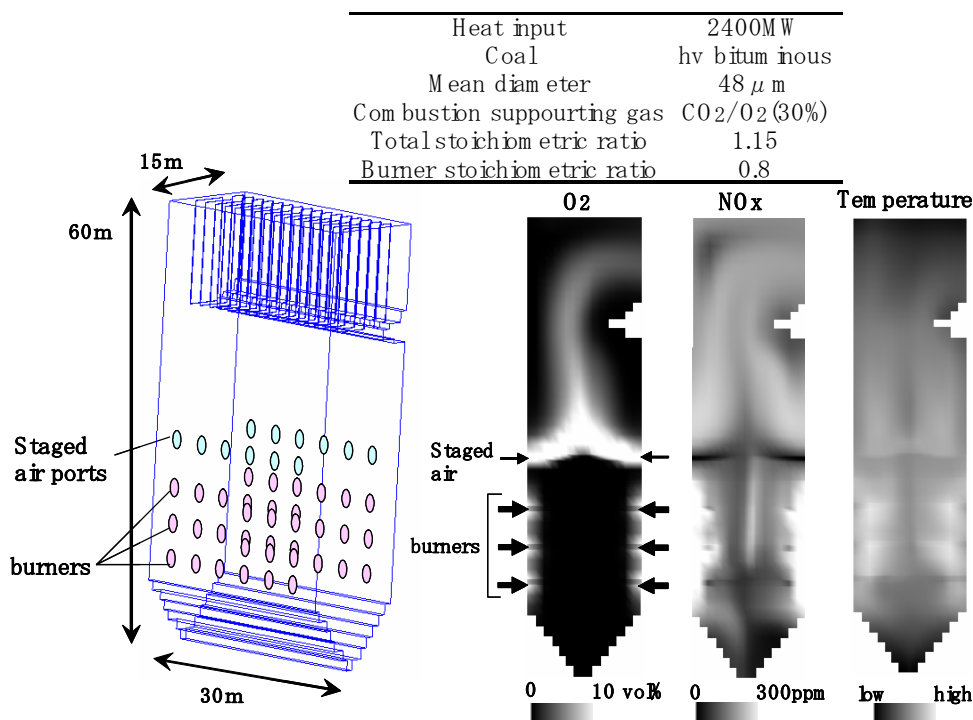
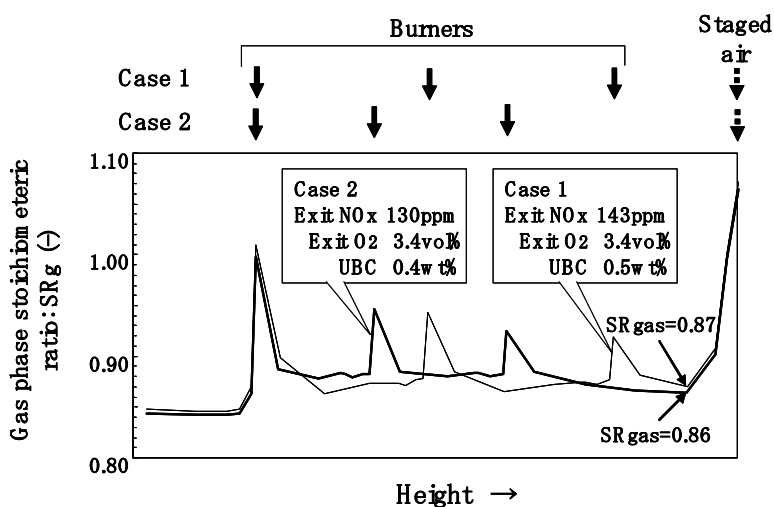


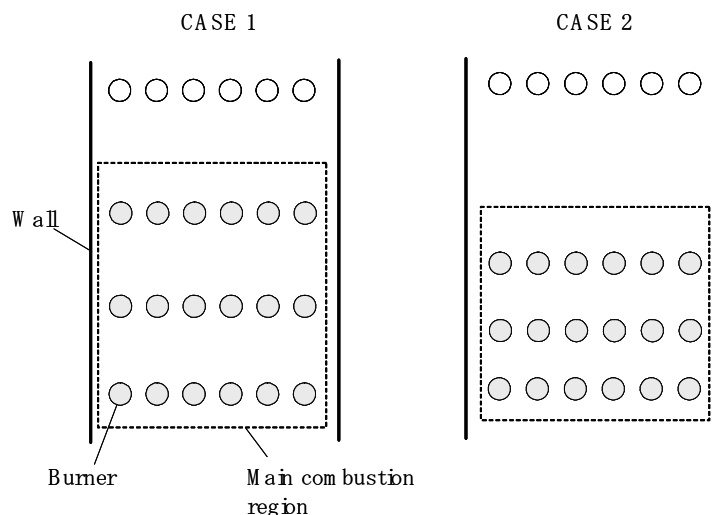
Figure 14. Distribution of calculated gas phase stoichiometric ratio.



The burner arrangements for CASE 1 and CASE 2 are described in Figure 15. Areas shown by dotted lines represent the main combustion region. Much of the supplied coal burned in this area. Much of the supplied heat was released in the area too. Total heat input of CASE 1 and CASE 2 were

the same, however, the main combustion region of CASE 1 was larger than that of CASE 2. Flame temperature in the main combustion region of CASE 2 was easy to increase, because heat was released in a small area. Oxidation and gasification reactions were accelerated for CASE 2, so that the corresponding SR_{gas} value was easy to decrease.

Figure 15. Arrangement of Burners for CASE 1 and CASE 2.

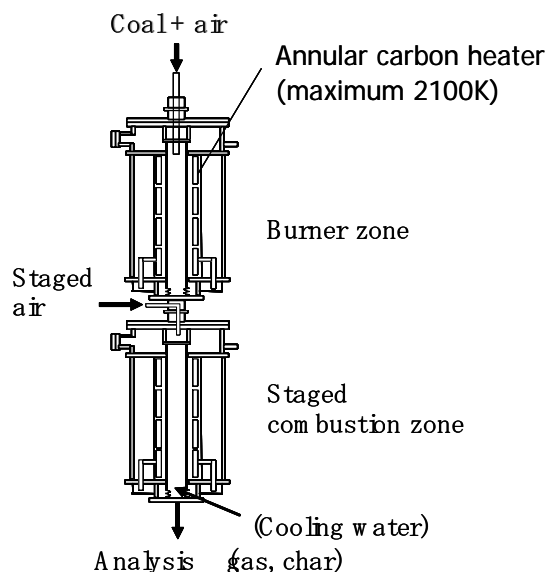


3. Experimental Section

The drop-tube furnace we used was described elsewhere [15]. The reaction zone (maximum length, 1200 mm) was made of an alumina tube which had an inner diameter of 50 mm. The heating rate was 15,000 K/s. The flow rate of combustion supporting gas (O_2/N_2) was $0.96 \text{ m}^3 \text{ N/h}$ and the supply rate of pulverized coals was 0.02–0.5 kg/h. A nozzle supplied the pulverized coals and combustion supporting gas to the furnace. The burning temperature (measured as the wall temperature) was 1173–1773 K. We changed the length (L) from the nozzle to a sampling port between 200, 400, and 800 mm. The reaction time was changed between approximately 0.25–1.0 s. Gas composition and ash content in unburned char were measured.

Staged combustion properties were also examined. The structure of the drop-tube furnace for staged combustion is shown in Figure 16. Two high-temperature electric furnaces were connected in series. The basic structure of the each drop-tube furnace was the same as described previously [15]. The maximum temperature was risen to 2100 K by using a carbon electric heater. Gasification reaction rates have been studied using a pressurized high-temperature drop-tube furnace [27]. We modified that the furnace to allow use at atmospheric pressure, and we used this design for the basic construction of our two electric furnaces. Coal and air (air for the burner zone) were supplied from the upper part of the electric furnace in the upper section. Coal was burnt under fuel-rich conditions in the upper electric furnace. Staged air was supplied at the connection of the two electric furnaces. The total amount of air (air for burner zone + staged air) was $0.96 \text{ m}^3 \text{ N/h}$.

Analyses of eleven coal samples are listed in Table 4. Five types were studied: sub-bituminous, hv-bituminous, mv-bituminous, and anthracite, and petroleum coke.

Figure 16. Structure of the drop-tube furnace for staged combustion.**Table 4.** Analysis of studied coals.

Name	Coal	Area	VM	Ash	Fuel	C	H	N	O	S	Mean Diameter (μm)
			(wt%, dry)		Ratio	(wt%, dry, ash-free)					
A	sub-bituminous	Asia	41.6	15.7	1.0	74.2	6.2	1.8	17.1	0.8	40
B	sub-bituminous	Noth America	43.6	6.2	1.2	69.1	5.4	1.1	23.8	0.6	23, 59, 155
C	hv-bituminous	Noth America	36.3	18.7	1.2	76.7	5.5	1.6	12.6	3.6	17
D	hv-bituminous	Oceania	31.1	14.9	1.7	81.1	5.8	1.8	10.7	0.7	37
E	hv-bituminous	Oceania	27.6	10.2	2.3	81.5	4.6	1.8	11.7	0.5	22
F	hv-bituminous	Oceania	26.3	12.8	2.3	84.9	5.5	1.9	7.2	0.5	14, 45
G	mv-bituminous	Oceania	20.6	8.5	3.4	87.6	4.7	2.1	4.8	0.8	40
H	petroleum coke	Noth America	11.8	2.4	7.3	88.7	3.3	1.5	1.3	5.4	33
I	anthracite	Asia	8.9	13.3	8.7	92.3	1.7	0.5	5.2	0.3	35
J	anthracite	Asia	7.6	25.3	8.8	90.7	3.5	1.4	3.5	1	16
K	hv-bituminous	Oceania	32.5	14.3	1.6	83.4	5.4	1.9	8.8	0.5	45

4. Conclusions

We applied a gas phase stoichiometric ratio index (SR_{gas}) to predict NO_x concentrations, to develop the NO_x reaction model and a new low- NO_x -combustion technology.

(1) Gas phase stoichiometric ratio (SR_{gas}) was defined as:

$$SR_{gas} = \text{amount of fuel required for stoichiometric combustion} / \text{amount of gasified fuel}$$

where the amount of gasified fuel was defined as the amount of fuel which had been released to the gas phase by pyrolysis, oxidation and gasification reactions. SR_{gas} was determined to be a good index to consider the gas phase reaction mechanism in fuel-rich pulverized coal flames.

(2) We applied the SR_{gas} index to develop a NO_x reaction model. The key feature was that the concentration of hydrocarbons was estimated as a function of SR_{gas} . Calculated NO_x

characteristics reproduced the experimental results obtained from a drop-tube furnace. The model was verified for various coals, particle diameters, reaction times and initial oxygen concentrations.

- (3) We applied *SRgas* to develop a low-NO_x-combustion system. When using staged combustion, it was important to reduce the *SRgas* value as much as possible, just before mixing with staged air. When we adopted the burner structure and the placement at which *SRgas* became the lowest, the NO_x emission of the furnace became the lowest as well.

References

1. Azuhata, A.; Narato, K.; Kobayashi, H.; Arashi, N.; Morita, S.; Masai, T. A study of gas composition profiles for low NO_x pulverized coal combustion and burner scale-up. *Proc. Combust. Inst.* **1986**, *21*, 1199–1206.
2. Förtsch, D.; Kluger, F.; Schnell, U.; Spliethoff, H.; Hein, K.R.G. A kinetic model for the prediction of NO emission from staged combustion of pulverized coal. *Proc. Combust. Inst.* **1998**, *27*, 3037–3044.
3. Cancès, J.; Commandrè, J.M.; Salvador, S.; Dagaut, P. NO reduction capacity of four major solid fuels in reburning conditions-Experiments and modeling. *Fuel* **2008**, *87*, 274–289.
4. Tsumura, T.; Morita, S.; Kiyama, K.; Kobayashi, H.; Yoshizako, H. Development of Extremely Low NO_x Pulverized Coal Burners by Using the Concept of “In-Flame NO_x Reduction”. In *Proceedings of JSME-ASME International Conference on Power Engineering-93*, Tokyo, Japan, 12–16 September 1993; Volume 2, pp. 325–330.
5. Taniguchi, M.; Kamikawa, K.; Okazaki, T.; Yamamoto, K.; Orita, H. A role of hydrocarbon reaction for NO_x formation and reduction in fuel-rich pulverized coal combustion. *Combust. Flame* **2010**, *157*, 1456–1466.
6. Williams, A.; Pourkashanian, M.; Bysh, P.; Norman, J. Modeling of coal combustion in low-NO_x p.f. flames. *Fuel* **1994**, *73*, 1006–1019.
7. Yamamoto, K., Fukuchi, T.; Chaki, M.; Shimogori, Y.; Matsuda, J. Development of Computer Program for Combustion Analysis in Pulverized Coal Fired Boilers. *Hitachi Rev.* **2000**, *49*, 4976–4980.
8. Yamamoto, K.; Taniguchi, M.; Kobayashi, H.; Sakata, T.; Kudo, K. Validation of coal combustion model by using experimental data of utility boilers. *JSME Int. J. Ser. B* **2005**, *48*, 571–578.
9. Le Bris, T.; Cadavid, F.; Caillat, S.; Pietrzyk, S.; Blondin, B.; Baudoin, B. Coal combustion modeling of large power plant, for NO_x abatement. *Fuel* **2007**, *86*, 2213–2220.
10. Man, C.K.; Gibbins, J.R.; Wikamp, J.G.; Zhang, J.; Schonenbeck, C.; Gadiou, R.; Schwartz, D. Coal characterization for NO_x prediction in air-staged combustion of pulverized coals. *Fuel* **2005**, *85*, 2190–2195.
11. Díez, L.I.; Cortés, C.; Pallarés, J. Numerical investigation of NO_x emission from a tangentially-fired utility boiler under conventional and overfire air operation. *Fuel* **2008**, *87*, 1259–1269.
12. Kambara, S.; Takarada, T.; Toyoshima, M.; Kato, K. Relation between functional forms of coal nitrogen and NO_x emissions from pulverized coal combustion. *Fuel* **1995**, *74*, 1247–1253.

13. Niksa, S.; Liu, G.S. Incorporating detailed reaction mechanisms into simulations of coal-nitrogen conversion in p.f. flames. *Fuel* **2002**, *81*, 2371–2385.
14. Bose, A.C.; Wendt, J.O.L. Pulverized coal combustion: fuel nitrogen mechanisms in the rich post-flame. *Proc. Combust. Inst.* **1998**, *22*, 1127–1134.
15. Taniguchi, M.; Yamamoto, K.; Kobayashi, H.; Kiyama, K. A reduced NO_x reaction model for pulverized coal combustion under fuel-rich conditions. *Fuel* **2002**, *81*, 363–371.
16. Chambrion, P.; Kyotani, T.; Tomita, A. C-NO reaction in the presence of O₂. *Proc. Combust. Inst.* **1998**, *27*, 3053–3059.
17. Aarna, I.; Suuberg, E.M. A study of the reaction order of the NO-carbon gasification reaction. *Proc. Combust. Inst.* **1998**, *27*, 3061–3068.
18. Guo, F.; Hecker, W.C. Kinetics of NO_x reduction by char: Effect of coal rank. *Proc. Combust. Inst.* **1998**, *27*, 3085–3092.
19. Schöonenbeck, C.; Gadiou, R.; Schwartz, D. A kinetic study of the high temperature NO-char reaction. *Fuel* **2004**, *83*, 443–450.
20. Yamamoto, K.; Murota, T.; Okazaki, T.; Taniguchi, M. Large eddy simulation of a pulverized coal jet flame ignited by a preheated gas flow. *Proc. Combust. Inst.* **2010**, *33*, 1771–1778.
21. Narato, K.; Kobayashi, H.; Taniguchi, M.; Kouno, T.; Okazaki, H.; Ito, K.; Morita, S.; Baba, A. Pulverized coal combustion burner. U.S. Patent 5685242, 11 November 1997.
22. Richardson M.; Shimogori, Y.; Kidera, Y. Supercritical Boiler Technology Matures. Available online: http://www.hitachipowersystems.us/supportingdocs/forbus/hpsa/technical_papers/CG2004.pdf (accessed on 14 March 2011).
23. Irie, K.; Sugauma, H.; Momoo, T., Komada, S.; Kojima, S. Commencement of the commercial operation of world's top performing 900MW unit “Maizuru No.1 thermal power station of the kansai electric power Co. Inc.”. *Mitsubishi Juko Giho* **2004**, *41*, 268–271
24. Kaneko, S.; Yamamoto, K.; Kinoshita, M.; Wakabayashi, Y.; Iida, Y. Design and Operation Experience of a 1000 MW Ultra Supercritical Coal Fired Boiler with Steam Condition of 25.4 Mpa 604/602 °C. *Mitsubishi Heavy Ind. Ltd. Tech. Rev.* **1999**, *36*, 61–65.
25. Yano, T.; Sakai, K.; Kiyama, K.; Okada, O.; Ochi, K. Updated low NO_x combustion technologies for boilers. Available online: http://www.hitachipowersystems.us/supportingdocs/forbus/hpsa/technical_papers/Mega2003.pdf (accessed on 14 March 2011).
26. Kimura, H.; Matsuda, J.; Sakai, K. Latest experience of coal fired supercritical sliding pressure operation boiler and application for overseas utilities. Available online: http://www.bhk.co.jp/english/technical/pdf/pge2003paper_blr.pdf (accessed on 17 March 2011).
27. Kajitani, S.; Hara, S.; Matsuda, H. Gasification rate analysis of coal char with a pressurized drop tube furnace. *Fuel* **2002**, *81*, 539–546.